

Strain dependence of the heat transport properties of graphene nanoribbons

Pei Shan Emmeline Yeo,^{1,2} Kian Ping Loh,¹ and Chee Kwan Gan^{2,*}

¹*Department of Chemistry, National University of Singapore, 3 Science Drive 3, Singapore 117543*

²*Institute of High Performance Computing, Agency for Science, Technology and Research, 1 Fusionopolis Way, #16-16 Connexis, Singapore 138632*

Using a combination of accurate density-functional theory and a nonequilibrium Green function's method, we calculate the ballistic thermal conductance characteristics of tensile-strained armchair (AGNR) and zigzag (ZGNR) edge graphene nanoribbons, with widths between 3 – 50 Å. The optimized lateral lattice constants for AGNRs of different widths display a three-family behavior when the ribbons are grouped according to N modulo 3, where N represents the number of carbon atoms across the width of the ribbon. Two lowest-frequency out-of-plane acoustic modes play a decisive role in increasing the thermal conductance of AGNR- N at low temperatures. At high temperatures the effect of tensile strain is to reduce the thermal conductance of AGNR- N and ZGNR- N . These results could be explained by the changes in force constants in the in-plane and out-of-plane directions with the application of strain. This fundamental atomistic understanding of the heat transport in graphene nanoribbons paves a way to effect changes in their thermal properties via strain at various temperatures.

PACS numbers: 68.65.-k, 66.70.-f, 63.20.D-

Keywords:

I. INTRODUCTION

Recently there is a surge in research activities on heat transport through nanostructures as evidenced by the emergence of a few review papers.^{1–3} The reasons for this change abound. The first is related to heat management in nanoelectronic circuits,⁴ since the miniaturization of electronic devices demands efficient dissipation of heat. The second is related to the utilization of the thermoelectric effect⁵ to harness heat in nanostructures that may help in alleviating the worldwide energy problem. Graphene and its derivatives such as graphene nanoribbons (GNRs) are among the most promising materials in these respects. Various experimental values for the heat conductivity of graphene have been reported, e.g., 4840 – 5300 Wm⁻¹K⁻¹ (Ref. 6), 600 – 630 Wm⁻¹K⁻¹ (Ref. 7), and 1400–2500 Wm⁻¹K⁻¹ (Ref. 8). This points to the fact that high heat conductivity is expected for graphene (in stark contrast to, e.g., the heat conductivity of Ag which is only ~ 430 Wm⁻¹K⁻¹ at room temperature). The high thermal conductance of graphene has made it very popular for use as a filler in thermal interface materials.³ For example, the heat conductivity of epoxy resins was improved by 30 times upon addition of 25 vol% graphene additive,⁹ and by 2.6 times when 2 wt% of graphene was added to polystyrene.¹⁰

Graphene could also be potentially used as a thermoelectric material to generate thermoelectric power.³ The efficiency of thermoelectric materials can be quantified using the thermoelectric figure of merit $ZT = S^2 G_e T / (\sigma_{el} + \sigma_{ph})$, where S is the Seebeck coefficient (also known as the thermopower), G_e is the electronic conductance, T is temperature and σ_{el} (σ_{ph}) is the electronic (thermal) conductance. Graphene has a superior¹¹ electronic conductance G_e , and a large¹² theoretical value of $S \sim 30$ mV/K. Even though the experimental¹³ val-

ues of S for graphene are more modest (40 – 80 μ V/K) compared to that for the inorganic^{5,14} thermoelectric materials (150 – 850 μ V/K), graphene might still qualify as a good thermoelectric material if its high value of $(\sigma_{el} + \sigma_{ph})$ could be suppressed. Although graphene is a semimetal, its heat conduction is dominated by σ_{ph} and not by σ_{el} due to the strong sp²-hybridization that efficiently transmits heat through lattice vibrations.¹⁵ Various ways have been proposed to increase the phonon scattering centers in graphene, e.g., by increasing the disorder at graphene edges,¹⁶ by introducing isotopes in graphene,¹⁷ and by creating vacancy defects in graphene.¹⁸ GNRs with vacancy defects was predicted to have a ZT of up to 0.25.¹⁹

The experimental demonstrations of the excellent heat properties of graphene and GNRs have stimulated many theoretical works.^{20–28} It is known that applying strain to graphene induces changes to the electronic structure,²⁹ resistance,³⁰ Raman spectra,³¹ and thermal conductivity³². For GNRs, different theoretical approaches have been used to study the heat properties of both the unstrained and strained GNRs. Thus far, molecular dynamics (MD) studies concluded that both compressive and tensile strains are detrimental to the heat conductivity of graphene³² or GNRs.^{24,25,33} Wei *et al.*²⁵ and Gunawardana *et al.*³³ concluded that the conductivity of armchair edge GNRs is more sensitive toward strain than their zigzag edge counterparts. Guo *et al.*²⁴ used a slightly different approach than that used in Ref. 25, which resulted in slightly different but essentially similar predictions. We note that the MD method is well-suited for investigating heat conduction in the diffusive regime and at high temperatures. However, in the ballistic regime and at low temperatures, intricate quantum mechanical effects come into play.²⁸ Since the phonon mean free path in graphene is ~ 775

nm at room temperature,⁴ the heat conduction is ballistic for small-scale graphene nanodevices. The phonon mean free path is reduced to ~ 20 nm in presence of edge disorders^{34,35}. Zhai *et al.*³⁶ addressed the thermal conductance of GNRs using a ballistic nonequilibrium Green's function (NEGF) approach.^{37–39} They extracted the force constants of strained graphene via the elasticity theory and applied that to study strained GNRs. They concluded that thermal conductance is enhanced with tensile strain, with an enhancement ratio of up to 17% and 36% for zigzag edge and armchair edge GNRs, respectively.³⁶ However, we note that a large 19% strain applied in Ref. 36 might put the applicability of the elasticity theory in the high strain regime to a severe test.

In this work, we investigate the thermal conductance characteristics of strained GNRs by using a combination of (1) density-functional theory (DFT) that accurately treats the atomic and electronic structures of subnanometer width GNRs, and (2) the NEGF method that has been extensively used to study the heat^{37,39} and electron⁴⁰ transport through nanostructures. Our results may shed light on how the heat conductivity of graphene-polymer composites could be affected under loading, and the possibility of using strain to tune the thermal conductance of GNRs to improve its ZT value.

II. MODELS AND METHODOLOGY

In this work, we calculate the thermal conductance of the zigzag (ZGNR- N) and armchair edge graphene nanoribbons (AGNR- N) as shown in Figure 1(a) using a combination of first-principles density-functional calculations and the ballistic nonequilibrium Green's function (NEGF) method.^{37–39,41} The uniaxial strain imposed on the GNRs is described by the strain parameter $\varepsilon = (\ell - \ell_0)/\ell_0$, where ℓ (ℓ_0) is the length (relaxed length) of the ribbon along the edges. A tensile (compressive) strain corresponds to $\varepsilon > 0$ ($\varepsilon < 0$). We note that the GNR edges have compressive edge stresses⁴² that might cause the GNRs to buckle^{43,44} that will lead to a decrease of thermal conductance^{24,25,32} due to increased phonon-phonon scattering. A proper treatment of buckled GNRs using DFT involves many atoms in a supercell and this demands extensive computing resources. Therefore we limit this work to studying the effects of tensile strain on the flat GNRs. The thermal conductance $\sigma(T, \varepsilon)$ at temperature T and strain ε is calculated from the Landauer expression,

$$\sigma(T, \varepsilon) = \int_0^\infty d\nu \, h\nu\theta(\nu) \frac{\partial n_B(\nu, T)}{\partial T} \quad (1)$$

or equivalently,⁴⁵

$$\sigma(T, \varepsilon) = \frac{h^2}{kT^2} \int_0^\infty d\nu \, \nu^2 \theta(\nu) \frac{e^{h\nu/kT}}{(e^{h\nu/kT} - 1)^2} \quad (2)$$

where $n_B(\nu, T) = \frac{1}{e^{h\nu/kT} - 1}$ is the Bose-Einstein distribution for frequency ν and temperature T , h (k) is

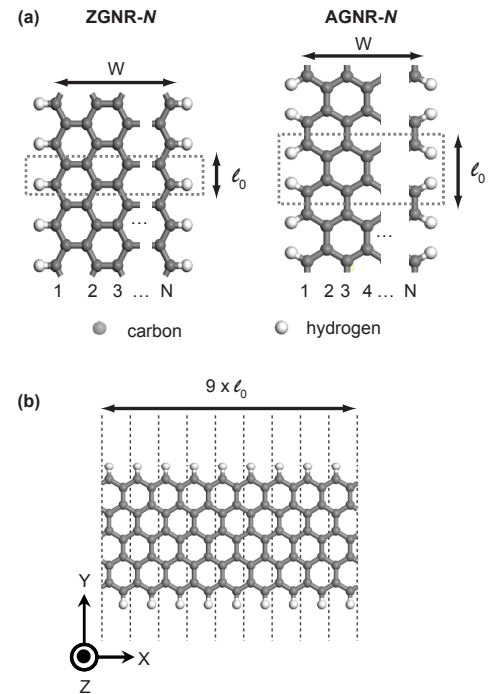


FIG. 1: (a) The width W of the zigzag (ZGNR- N) and armchair (AGNR- N) edge graphene nanoribbons is controlled by N that represents the number of carbon atoms across the width of the ribbon. Hydrogen atoms are attached to the edge carbon atoms to terminate the dangling bonds. For very large W , the optimized length ℓ_0 of the primitive cell along the edge direction should approach a'_0 for ZGNR- N and $a'_0\sqrt{3}$ for AGNR- N , where a'_0 is the lattice parameter of graphene. The primitive unit cells are demarcated by dotted lines. (c) A supercell comprising of nine primitive unit cells is constructed for the phonon calculations.

the Planck (Boltzmann) constant. The key quantity is the transmission function $\theta(\nu)$ that may be calculated in general cases using the nonequilibrium Green's function method³⁸ or by counting the number of phonon bands at frequency ν for quasi-one-dimensional periodic systems.⁴⁵ We have used the latter approach to get $\theta(\nu)$ due to its computational efficiency to treat the problem at hand. It is interesting to note that at low temperatures T , only the very low-frequency modes contribute to thermal conductance. Therefore $\theta(\nu \rightarrow 0) = N_m$ in eqn. 2 may be taken out of the integral sign and this leads to a quantization^{46,47} of the thermal conductance according to $\sigma(T, \varepsilon) = \frac{k^2 T}{h} N_m \int_0^\infty du \frac{u^2 e^u}{(e^u - 1)^2} = N_m \frac{\pi^2 k^2 T}{3h}$.

We perform density-functional theory (DFT) calculations using the SIESTA package.⁴⁸ The local-density approximation is used for the exchange-correlation functional. Double- ζ basis sets and Troullier-Martins pseudopotentials are used for the C and H atoms. We use a vacuum separation of 15 Å in the y and z directions consistent with the convention adopted in Figure 1(b). The mesh cutoff is 400 Ry. The atomic positions are relaxed using the conjugate gradient algorithm with a force

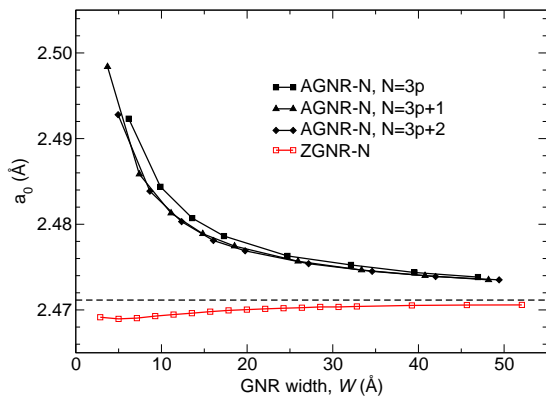


FIG. 2: The approach of the optimized lateral lattice parameter a_0 for AGNR- N ($N = 4$ to 41) and ZGNR- N ($N = 2$ to 25) toward a'_0 , the optimized lattice parameter of graphene (denoted by a horizontal dash line) as the width W of the ribbon increases. A three-family behavior is observed for AGNR- N .

tolerance criterion of 10^{-3} eV/Å. As was demonstrated in Refs. 49 and 42, spin-polarization effects are particularly important for ZGNRs. Therefore we perform spin-polarized (nonspin-polarized) calculations for ZNGR- N (AGNR- N).

Phonon dispersion relations of GNRs are calculated using the supercell method.^{50–52} To minimize interactions from the distant periodic images of a displaced atom from its equilibrium position, a supercell of nine primitive cells sufficient for this purpose is used.²⁸ We displace the i th atom in a primitive cell from its equilibrium position by $\pm\delta_{i\alpha} = \pm 0.015$ Å and evaluate the forces acting on the j th atom in the supercell $F_{j\beta}(\pm\delta_{i\alpha})$ using the Hellmann-Feynman theorem. α and β denote the Cartesian directions. We then use a finite central-difference scheme to evaluate the matrix elements of the force constant matrix K , where $K_{i\alpha, j\beta} = \frac{\partial^2 E}{\partial r_{i\alpha} \partial r_{j\beta}} = - \left[\frac{F_{j\beta}(+\delta_{i\alpha}) - F_{j\beta}(-\delta_{i\alpha})}{2\delta_{i\alpha}} \right]$. To reduce the number of static DFT calculations, we exploit the space group operations of AGNR- N and ZGNR- N so that only atoms in the inequivalent positions are displaced. The forces⁵⁰ or interatomic force constants on the equivalent atoms are deduced from that of the inequivalent atoms. AGNR- N with $N = 2(p+1)$ and $N = 2p+1$ belong to the space group number 51 and 47, respectively, where $p \geq 1$ is a positive integer; while ZGNR- N with $N = 2p$ and $N = 2p+1$ belong to the space group number 47 and 51, respectively. The unstrained (strained) graphene belongs to the space group number 191 (65).

III. RESULTS AND DISCUSSION

A. Optimized Lattice Parameter of GNRs

Since this work concerns the effect of strain $\varepsilon = (\ell - \ell_0)/\ell_0$ on the thermal conductance, we first need to obtain the optimized length ℓ_0 (see Figure 1) of GNR- N for different N (or equivalently, width W). We obtain ℓ_0 for each N by performing atomic relaxation of GNRs with different ribbon lengths ℓ in the x direction (see Figure 1). The total energies of the relaxed structures are then fitted to a polynomial function to obtain the optimized ribbon length ℓ_0 . For ease of comparison between AGNR- N and ZGNR- N , the optimized lateral lattice parameter a_0 is calculated according to $a_0 = \frac{\ell_0}{\sqrt{3}}$ and $a_0 = \ell_0$ for AGNR- N and ZGNR- N respectively. From Figure 2, we find that while a_0 for ZGNR- N monotonically increases toward $a'_0 = 2.471$ Å (the optimized lattice parameter of graphene) with increasing W , a_0 of AGNR- N monotonically decreases toward a'_0 with an observation that AGNR- N exhibits a three-family behavior for a_0 , i.e., the convergence of a_0 is systematic when the AGNR- N are grouped according to N modulo 3. We note that other three-family behaviors for AGNR- N have also been found for the electronic bandgap⁴⁹, edge energy^{42,53}, and the LO/TO splitting⁵⁴. The three-family behavior for a_0 of the AGNR- N ribbons may be understood using the concepts of aromaticity and resonance bond theory.⁵⁵ Wassmann *et al.* argued that AGNRs can be classified into three different families depending on the number of equivalent Clar's structures that can be constructed for each AGNR- N .⁵³ Clar's structures must contain the maximum number of aromatic π -sextets which can be accommodated by the structure. In Figure 3, we show examples of the equivalent Clar's structure that can be constructed for AGNR- N belonging to the three different families, and the bond lengths for the optimized structures. For AGNR- N where $N = 3p$ and p is an integer, only one Clar's structure can be constructed; for $N = 3p+1$, there are two equivalent Clar's structures, and for $N = 3p+2$, more than two equivalent Clar's structures can be constructed. Since the C-C resonance bond is shorter than the C-C single bond, the $N = 3p$ structures will have longer bond lengths – which results in a larger a_0 – as compared to the $N = 3p+1$ and $N = 3p+2$ structures. In contrast, for ZGNR- N with unpaired spins at the edges, more than two equivalent Clar's structure can be drawn for any N .⁵³ For width $W \sim 50$ Å, the value of a_0 differs from that of the bulk graphene by less than 0.1% (0.02%) for AGNR- N (ZGNR- N).

B. Thermal Conductance of Unstrained GNRs

Using the optimized ℓ_0 and atomic coordinates for GNR- N , we perform the phonon dispersion calculation

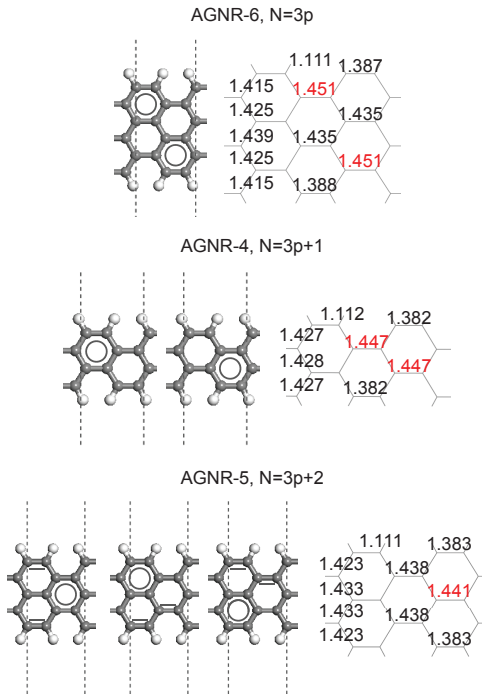


FIG. 3: The three families of AGNR- N : the $N = 3p$ family has only one possible Clar’s structure, the $N = 3p + 1$ family has two Clar’s structures and the $N = 3p + 2$ family has more than two Clar’s structures. The bond lengths for each optimized AGNR are also shown. The longest C–C bonds in each structure are highlighted in red.

(see Figure 6 for typical results) and subsequently obtain the thermal conductance by the counting method⁴⁵. Figure 4(a) shows the thermal conductance $\sigma(T, \varepsilon)$ at $T = 300$ K and $\varepsilon = 0.00$ for GNRs as a function of W . We find that ZGNR- N have higher conductances as compared to AGNR- N with comparable W . This is due to the fact that the phonon dispersions of ZGNR are more dispersive (a single phonon branch is more dispersive if it covers a larger frequency range) compared to that of AGNRs,²⁸ thus increasing the thermal conductance through a change in the transmission function $\theta(\nu)$. Since the dispersiveness is related to the gradient $d\omega/dk$, which is the phonon velocity,⁴⁶ we may also say that ZGNRs have higher phonon velocities than AGNRs, resulting in higher thermal conductance.

While bulk graphene is a fully π -resonant structure with equal C–C bond lengths between the C atoms, the presence of edges in the GNRs limits the extent of the π -resonance. Hence not all of the C–C bond lengths are equivalent as explained in Figure 3. Therefore, we expect the thermal conductance of GNRs to be different from bulk graphene due to this edge effect. In Figure 4(b), we show the average transmission function $\theta(\nu)$ for the bulk graphene in the armchair and zigzag directions. The $\sigma(300$ K, 0.00) for bulk graphene in the armchair (zigzag) direction is 0.18 nW/K (0.32 nW/K). As $W \rightarrow \infty$, the

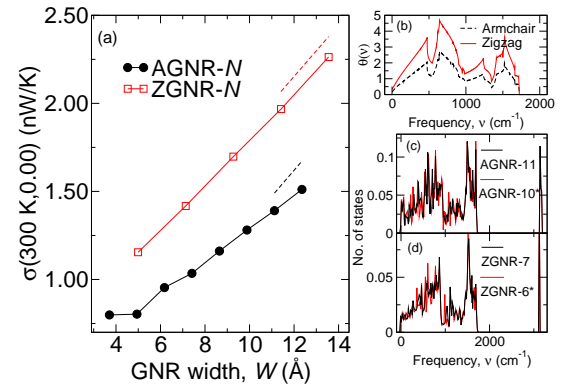


FIG. 4: (a) Thermal conductance $\sigma(T = 300$ K, $\varepsilon = 0.00$) of AGNR- N ($N = 4$ to 11) and ZGNR- N ($N = 3$ to 7). The slopes of the dash lines are deduced from the thermal conductance of bulk graphene at 300 K in the armchair and zigzag directions. (b) Average transmission function for bulk graphene along the armchair and zigzag directions. (c) Phonon densities of states (DOS) of AGNR-11 and AGNR-10*, which is the sum of the DOS of AGNR-10 and the DOS of bulk graphene. (d) Phonon DOS of ZGNR-7 and ZGNR-6*, which is the sum of the DOS of ZGNR-6 and the DOS of bulk graphene.

edge effect of GNRs should converge to some finite value, and hence the conductance increase from AGNR- $(N - 1)$ to AGNR- N should approach the conductance value of bulk graphene in the armchair direction. The expected conductance slopes for AGNRs and ZGNRs are shown in Figure 4(a). Table ?? shows that for the largest W investigated in this study — AGNR-11 and ZGNR-7 — the conductance slope for AGNR-11 is 34% lower than that predicted for the bulk graphene, whereas the slope is only 5% lower for ZGNR-7. These discrepancies may be attributed to the strong edge effect on the narrow width ribbons that we have studied here. Even though we are unable to provide a quantitative measure of the edge effects, we are able to provide qualitative evidence of the edge effect. In Figure 4(c), we show the phonon density of states (DOS) for AGNR-11 and AGNR-10*, which is sum of the DOS of AGNR-10 and the DOS of bulk graphene. We find that the edge effect is still rather strong in the GNRs since the DOS of AGNR-11 does not match well with AGNR-10*. Similarly the DOS of ZGNR-7 does not match well with ZGNR-6*. This in turn suggests why the conductance slopes do not agree for very narrow width ribbons. We point out the fact that ZGNR- N has a better agreement in the conductance slope compared to AGNR- N is consistent with the observation that a_0 converges faster to a'_0 (the optimized lattice parameter of graphene) for ZGNR- N than for AGNR- N , as shown in Figure 2.

It is found that, except for AGNR-3, all unstrained ZGNR- N and AGNR- N are stable when l_0 corresponds to a'_0 and $a'_0\sqrt{3}$, respectively, with a small adjustment according to Figure 2. Figure 5(b) shows the phonon dispersion of AGNR-3 (more commonly known as

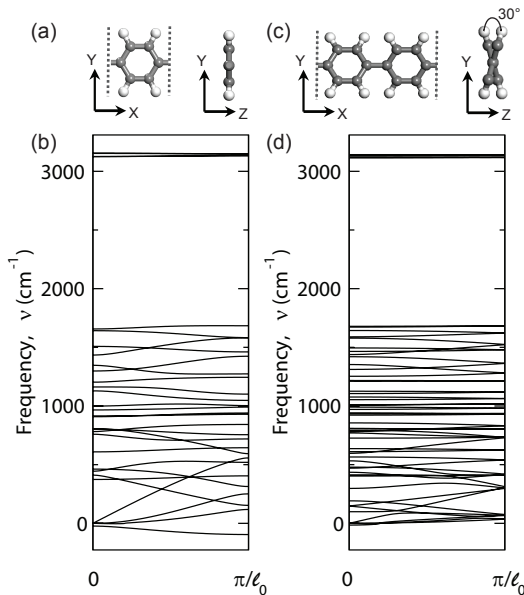


FIG. 5: The primitive cell of AGNR-3 (a) shows a large negative frequency of $\sim 100 \text{ cm}^{-1}$ in the phonon dispersion relations at the zone boundary (b). The relaxed structure (c) of the enlarged primitive cell AGNR-3, where the torsion angle between the 2 hexagon rings is 30° . (d) Phonon dispersion relation of the enlarged primitive cell of AGNR-3 shows no soft modes.

polyphenylene) of a 10-atom primitive cell that possesses soft modes extending from Γ point to the zone boundary with a large negative frequency of $\sim 100 \text{ cm}^{-1}$. We create a new 20-atom supercell by combining two adjacent primitive cells along the x direction, which causes the soft mode of the original supercell at the zone boundary to be folded to Γ point of the Brillouin zone of the enlarged supercell. We perform a phonon calculation for the 20-atom supercell and use the eigenvector of the lowest frequency (i.e., the eigenmode with imaginary frequency) to displace the atoms for a further atomic relaxation. We obtain a relaxed structure shown in Figure 5(c), where a torsion angle of 30° between alternate hexagon rings is observed. This is slightly smaller than the 40° calculated by Brocorens *et al.* using the Hartree-Fock AM1 method for terphenyl.⁵⁶ The enlarged supercell for AGNR-3 is indeed stable according to the phonon dispersion relation shown in Figure 5(d), where no soft modes are observed. This unit cell has a lower total energy of 4 meV/atom compared to that of the unstable, planar AGNR-3.

C. Effect of Tensile Strain on Thermal Conductance of GNRs

Next we investigate the effect of tensile strain on the thermal conductance of GNRs. Two different strain values $\epsilon = 0.05$ and 0.10 have been applied to the GNRs.

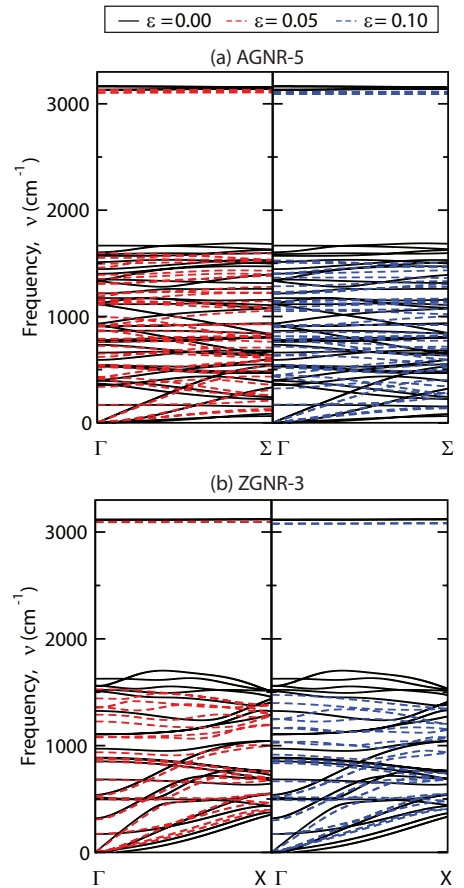


FIG. 6: Phonon dispersion relations for (a) AGNR-5 and (b) ZGNR-3. Three different strain values of $\epsilon = 0.00, 0.05,$ and 0.10 are considered.

Similar to the previous section, we perform phonon calculations for AGNR- N and ZGNR- N before we calculate the thermal conductance. Figure 6 shows the typical phonon dispersion relations for AGNR-5 and ZGNR-3. We see that while the highest-frequency C-H stretching modes of $\sim 3200 \text{ cm}^{-1}$ are not affected by strain, all other high-frequency modes between $\sim 1000 - 1600 \text{ cm}^{-1}$ are consistently reduced. On the other hand, the two lowest-frequency out-of-plane acoustic (ZA) modes increase in frequency as strain is applied. (In the case of graphene, Bonini *et al.* observed that the frequency of the out-of-plane mode increases as isotropic tensile strain is applied.⁵⁷) The changes to the eigenmode frequencies may be understood from the changes to the force constants as strain is applied, as shown in Figure 7 (to simplify analysis, we show only the $xx, yy,$ and zz diagonal components). Tensile strain in AGNR-5 leads to substantial decrease in the in-plane force constants along the longitudinal (x) and transverse (y) directions due to the lengthened C-C bonds.^{58,59} The largest decrease in the force constants for AGNR-5 is -24% and -10% in the xx and yy directions, respectively. For ZGNR-3, the largest decrease is -42% and -13% in the xx and yy compo-

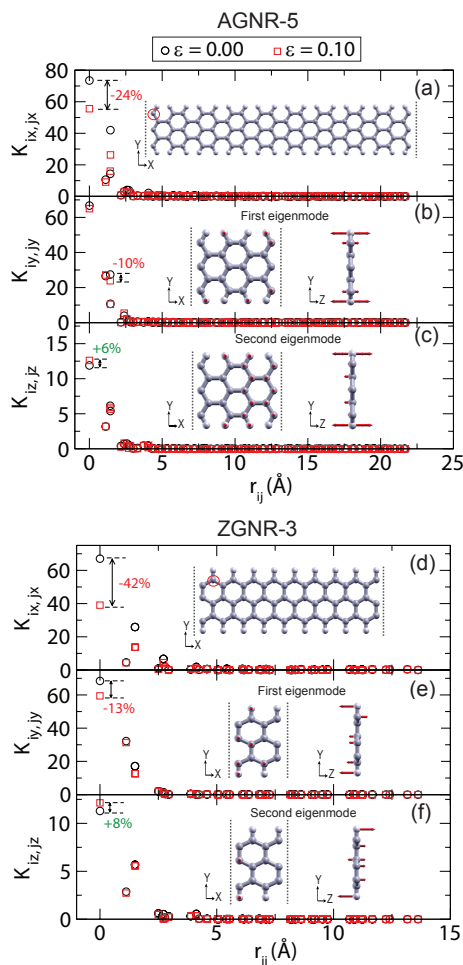


FIG. 7: The force constant $K_{i\alpha,j\alpha}$ (in units $\text{eV}/\text{\AA}^2$) of AGNR-5 as a function of $r_{ij} = |\mathbf{r}_i - \mathbf{r}_j|$ for the i th (j th) atom located at \mathbf{r}_i (\mathbf{r}_j). The i th atom (circled in red in the inset of (a)) is displaced in (a) $\alpha = x$, (b) $\alpha = y$, and (c) $\alpha = z$ direction. The strain values are $\varepsilon = 0.00$ (black circles) and $\varepsilon = 0.10$ (red squares). The two lowest out-of-plane (ZA) phonon eigenmodes are depicted in the insets of (b) and (c). The arrows (in red) on the atoms indicate the vibration direction and amplitude of each atom. The results in (d–f) are for ZGNR-3.

nents, respectively. However, the force constants in the out-of-plane (z) direction have either increased slightly or remained the same, and this leads to the increase of the frequency of the out-of-plane modes. The largest increase in the force constants in the zz component is 6% (8%) for AGNR-5 (ZGNR-3).

The effect of strain on the thermal conductance is shown in Figure 8 for three representative temperatures $T = 50$ (low temperature), 300 (intermediate temperature) and 500 K (high temperature). To directly compare the conductance of a strained GNR and an unstrained GNR, we define the relative conductance as $\sigma_r(T, \varepsilon) = \frac{\sigma(T, \varepsilon)}{\sigma(T, 0)}$. The results for $\sigma_r(T, \varepsilon)$ are shown in Figure 9.

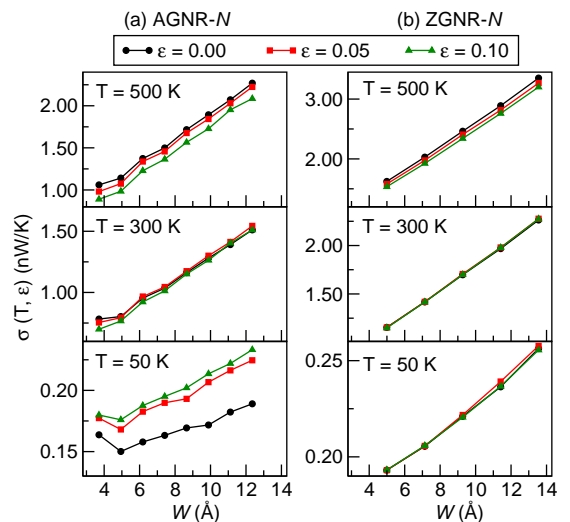


FIG. 8: Conductance plots for (a) AGNR- N ($N = 4$ to 11) and (b) ZGNR- N ($N = 3$ to 7) for $\varepsilon = 0.00, 0.05$ and 0.10 and $T = 50, 300$ and 500 K.

We find that at a low temperature of $T = 50$ K, the thermal conductance is dominated by the low-frequency modes²⁸ since the derivative $\frac{\partial n_B}{\partial T}$ diminishes rapidly with increasing ν . For AGNR- N , the thermal conductance substantially increases when tensile strain is applied, where an increase of up to 20% compared to the unstrained AGNR can be achieved. This increase in conductance is due to an increase in the frequencies of the two lowest-frequency acoustic phonon eigenmodes upon the application of strain, as was discussed in Figure 6(a).

However for ZGNR- N at $T = 50$ K, $\sigma_r(T, \varepsilon)$ with $\varepsilon = 0.05$ and 0.10 does not increase, but remains fairly constant at 1, despite the fact that the lowest-frequency out-of-plane ZA modes also increase in frequency after strain is applied. This is because the two low-frequency out-of-plane ZA phonon eigenmodes of unstrained ZGNR- N are more dispersive than AGNR- N (e.g., the frequency at the zone boundary is 370 cm^{-1} for ZGNR-3 versus 90 cm^{-1} for AGNR-5, as shown in Figure 6), even though the frequencies of the lowest two ZA phonon branches increase with strain. Hence we can understand that the increase of thermal conductance in AGNR- N is due to the presence of new low-frequency modes that are easily excited at a low temperature. For ZGNR- N , a low temperature only excite the existing low-frequency modes because the new low-frequency modes (from the effect of strain) occur at much higher frequencies as compared to that of the AGNR- N , and therefore cannot be easily excited thermally. Our results at low temperature differ from that reported in Ref. 36 where essentially the same increase in thermal conductance occurs for both AGNR- N and ZGNR- N . As the temperature increases, the higher-frequency modes start to contribute to the thermal conductance in addition to the lower-frequency ones. However, since the high-frequency modes are suppressed due to the smaller force constants caused by the lengthening

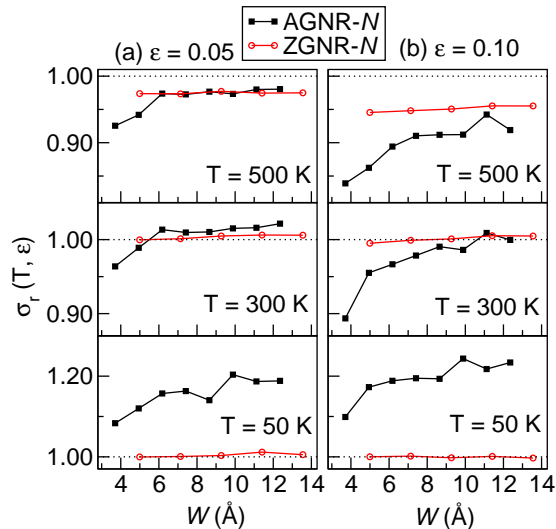


FIG. 9: Relative conductance $\sigma_r(T, \epsilon)$ of AGNR- N ($N = 4$ to 11) and ZGNR- N ($N = 3$ to 7) of width W for (a) $\epsilon = 0.05$ and (b) $\epsilon = 0.10$ for at $T = 50, 300$ and 500 K.

of the strained bonds, there will be competition between the reduction in thermal conductance due to the high-frequency modes, and the increase due to low-frequency modes. For AGNR- N at $T = 300$ and 500 K, the former effect is stronger than the latter, especially at a larger strain value, and this explains the significant reduction of the thermal conductance as shown in Figure 8(a) at progressively higher temperatures. However, for ZGNR- N , the effects of high- and low-frequency almost cancel out each other, thus leading to a near-constant behavior of thermal conductance. From Table ??, we see that the edge effect is generally stronger for AGNRs than for ZGNRs even in the presence of strain.

Since the thermal conductance of the GNRs displays a nonmonotonic behavior with temperature, it may be useful to discuss the ‘cross-over temperature’ of the GNRs, which is the temperature below (above) which the thermal conductance of a strained GNR is more (less) than that of the unstrained GNR. We show in Figure 10 the cross-over temperatures of the strained GNRs, and note that they are close to room temperature. This shows that we may control the thermal conductance of strained GNRs within a reasonable range of temperatures.

Finally we also investigate the relative conductance of a few GNRs at different strain values, the results of which are shown in Figure 11. At low temperatures such as $T = 50$ K, the thermal conductance of AGNR- N increases monotonically with increasing ϵ ; whereas it remains fairly constant for ZGNR- N . At higher temperatures of $T = 300$ and 500 K, $\sigma_r(T, \epsilon)$ for both AGNR- N and ZGNR- N decrease with increasing ϵ , with AGNR- N showing a larger relative drop for the same amount of ϵ . We find that the thermal conductance of AGNRs is more sensitive to tensile strain than ZGNRs at 300 K, which is consistent with the conclusions of Wei *et al.*²⁵ Zhai

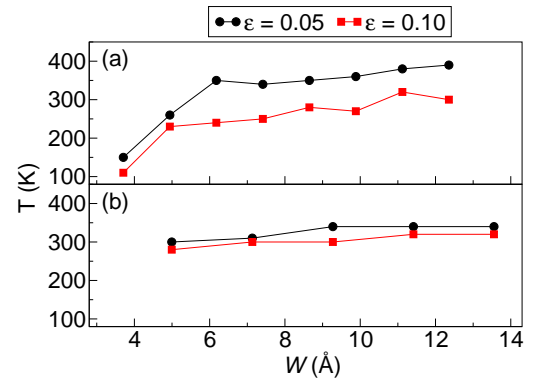


FIG. 10: Cross-over temperatures (see text) for (a) AGNR- N ($N = 4$ to 11) and (b) ZGNR- N ($N = 3$ to 7) at $\epsilon = 0.05$ and 0.10 .

*et al.*³⁶ predicted that with the application of $\epsilon = 0.19$ on GNRs of wide widths (~ 2.6 nm), the thermal conductance of strained GNRs should be higher than the corresponding unstrained ones even at 400 K. In the case of the narrow width GNRs studied in this paper, we show in Figure 10 that the cross-over temperatures do not exceed 400 K. We attribute the discrepancy between our results and those obtained by Zhai *et al.* due to their assumptions that the out-of-plane elastic constants do not change with strain and that only nearest-neighbor force constants are used. Recently, significant progress has been made toward synthesizing GNRs of specific edge orientations.⁶⁰ Based on our results, we predict that the thermal conductance anisotropy between AGNRs and ZGNRs suggests selective use of ZGNRs as fillers in thermal interface materials because their thermal conductance is higher and less adversely affected by strain as compared to AGNRs. AGNRs on the other hand, might act as a suitable thermoelectric material because of their inherent lower thermal conductance compared to ZGNRs, and their thermal conductance can be further lowered with the application of strain. However, the nonmonotonic variation of thermal conductance with respect to strain for the AGNRs means that straining the AGNRs to decrease their thermal conductance shall only be effective above the cross-over temperature.

IV. CONCLUSION

In conclusion, we have investigated the thermal conductance of AGNR- N and ZGNR- N as a function of tensile strain on the GNRs with accurate density-functional theory calculations and the nonequilibrium Green’s function method. The lateral lattice constants of AGNR- N are found to follow a three-family behavior that depends on N . We found that tensile strain decreases the force constants in the in-plane directions of the GNRs, but slightly increases the force constants in the out-of-plane direction, which increase the two lowest-frequency out-

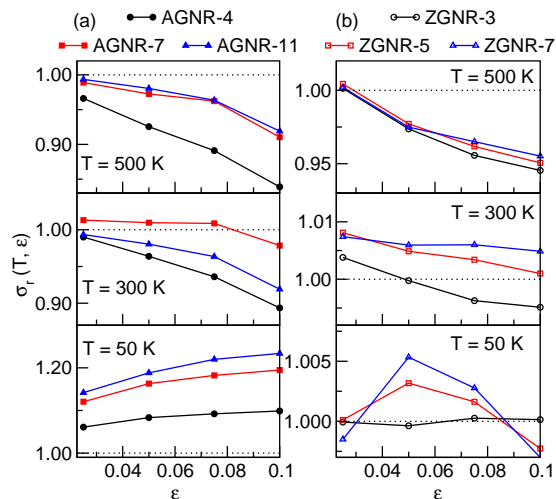


FIG. 11: Relative conductance $\sigma_r(T, \epsilon)$ versus strain ϵ for (a) AGNR- N ($N = 4, 7,$ and 11) and (b) ZGNR- N ($N = 3, 5,$ and 7) at $T = 50, 300$ and 500 K.

of-plane acoustic modes. These modes play a decisive role in increasing the thermal conductance of AGNR- N at low temperatures, but not for ZGNR- N . Hence the fact that the phonon dispersions of ZGNR- N is more dispersive than that of AGNR- N of comparable widths results in two important outcomes: (1) the unstrained

ZGNR- N has a higher thermal conductance compared to the unstrained AGNR- N of comparable widths, and (2) that at low temperatures, the thermal conductance of the strained ZGNR- N is less sensitive toward the effect of strain than that of AGNR- N . At high temperatures, the thermal conductance of the strained ZGNR- N and AGNR- N decreases (relative to the unstrained ones) with strain due to the fact that the frequency of the high-frequency modes shifts down as a result of the weakening of the interatomic force constants in the in-plane direction. The use of the state-of-the-art techniques such as density-functional theory and the nonequilibrium Green's function method is able to reveal intricate quantum-mechanical effects that may be hard or impossible to be captured with force-field type interactions. Finally, it might be interesting to study the role of out-of-plane modes in other strained single-layer systems such BN, MoS₂, and WSe₂.

Acknowledgements

The authors gratefully acknowledge useful discussions with Jian-Sheng Wang, Zhen Wah Tan and Jinghua Lan. We acknowledge the support of A*STAR Computational Resource Center (A*CRC) of Singapore.

* Electronic address: ganck@ihpc.a-star.edu.sg

- ¹ Y. Dubi and M. DiVentra. Colloquium: Heat flow and thermoelectricity in atomic and molecular junctions. *Rev. Mod. Phys.*, 83:131, 2011.
- ² Jian -S Wang, J. Wang, and J. T. Lü. Quantum thermal transport in nanostructures. *Eur. Phys. J. B*, 62(4):381, 2008.
- ³ Alexander A. Balandin. Thermal properties of graphene and nanostructured carbon materials. *Nat. Mater.*, 10(8):569, 2011.
- ⁴ S. Ghosh, I. Calizo, D. Teweldebrhan, E. P. Pokatilov, D. L. Nika, A. A. Balandin, W. Bao, F. Miao, and C. N. Lau. Extremely high thermal conductivity of graphene: Prospects for thermal management applications in nano-electronic circuits. *Appl. Phys. Lett.*, 92(15):151911, 2008.
- ⁵ T. C Harman, P. J Taylor, M. P Walsh, and B. E LaForge. Quantum dot superlattice thermoelectric materials and devices. *Science*, 297(5590):2229, 2002.
- ⁶ A. A. Balandin, S. Ghosh, W. Bao, I. Calizo, D. Teweldebrhan, F. Miao, and C. N. Lau. Superior thermal conductivity of single-layer graphene. *Nano Lett.*, 8:902, 2008.
- ⁷ Clement Faugeras, Blaise Faugeras, Milan Orlita, M. Potemski, Rahul R. Nair, and A. K. Geim. Thermal conductivity of graphene in corbino membrane geometry. *ACS Nano*, 4(4):1889, 2010.
- ⁸ Weiwei Cai, Arden L. Moore, Yanwu Zhu, Xuesong Li, Shanshan Chen, Li Shi, and Rodney S. Ruoff. Thermal transport in suspended and supported monolayer graphene grown by chemical vapor deposition. *Nano Lett.*,

- 10(5):1645, 2010.
- ⁹ Aiping Yu, Palanisamy Ramesh, Mikhail E. Itkis, Elena Bekyarova, and Robert C. Haddon. Graphite Nanoplatelets/Epoxy composite thermal interface materials. *J. Phys. Chem. C*, 111(21):7565, 2007.
- ¹⁰ Ming Fang, Kaigang Wang, Hongbin Lu, Yuliang Yang, and Steven Nutt. Single-layer graphene nanosheets with controlled grafting of polymer chains. *J. Mater. Chem.*, 20(10):1982, 2010.
- ¹¹ K I Bolotin, K J Sikes, J Hone, H L Stormer, and P Kim. Temperature-Dependent transport in suspended graphene. *Phys. Rev. Lett.*, 101(9):096802, 2008.
- ¹² D. Dragoman and M. Dragoman. Giant thermoelectric effect in graphene. *Appl. Phys. Lett.*, 91:203116, 2007.
- ¹³ Peng Wei, Wenzhong Bao, Yong Pu, Chun Ning Lau, and Jing Shi. Anomalous thermoelectric transport of dirac particles in graphene. *Phys. Rev. Lett.*, 102(16):166808, 2009.
- ¹⁴ Kuei Fang Hsu, Sim Loo, Fu Guo, Wei Chen, Jeffrey S Dyck, Ctirad Uher, Tim Hogan, E. K Polychroniadis, and Mercouri G Kanatzidis. Cubic AgPbmSbTe_{2+m}: bulk thermoelectric materials with high figure of merit. *Science*, 303(5659):818, 2004.
- ¹⁵ P. G. Klemens. Theory of the A-plane thermal conductivity of graphite. *J. Wide Bandgap Mater.*, 7(4):332, 2000.
- ¹⁶ Alexander V. Savin, Yuri S. Kivshar, and Bambi Hu. Suppression of thermal conductivity in graphene nanoribbons with rough edges. *Phys. Rev. B*, 82(19):195422, 2010.
- ¹⁷ Jiuning Hu, Stephen Schiffl, Ajit Vallabhaneni, Xiulin Ruan, and Yong P Chen. Tuning the thermal conduc-

- tivity of graphene nanoribbons by edge passivation and isotope engineering: A molecular dynamics study. *Appl. Phys. Lett.*, 97(13):133107, 2010.
- 18 J. Haskins, A. Kinaci, Cem Sevik, H. Sevincli, G. Cuniberti, and T. Cagin. Control of thermal and electronic transport in defect-engineered graphene nanoribbons. *ACS Nano*, 5:3779, 2011.
 - 19 Tue Gunst, Troels Markussen, A. -P. Jauho, and Mads Brandbyge. Thermoelectric properties of finite graphene antidot lattices. *Phys. Rev. B*, 84(15):155449, 2011.
 - 20 S. Ghosh, D. L. Nika, E. P. Pokatilov, and A. A. Balandin. Heat conduction in graphene: experimental study and theoretical interpretation. *New J. Phys.*, 11:095012, 2009.
 - 21 D. L. Nika, E. P. Pokatilov, A. S. Askerov, and A. A. Balandin. Phonon thermal conduction in graphene: Role of umklapp and edge roughness scattering. *Phys. Rev. B*, 79:155413, 2009.
 - 22 J. Lan, J. -S. Wang, C. K. Gan, and S. K. Chin. Edge effects on quantum thermal transport in graphene nanoribbons: Tight-binding calculations. *Phys. Rev. B*, 79:115401, 2009.
 - 23 Zhong Xiang Xie, Ke Qiu Chen, and Wen Hui Duan. Thermal transport by phonons in zigzag graphene nanoribbons with structural defects. *J. Phys.: Condens. Matter*, 23:315302, 2011.
 - 24 Z. X. Guo, D. E. Zhang, and X. G. Gong. Thermal conductivity of graphene nanoribbons. *Appl. Phys. Lett.*, 95:163103, 2009.
 - 25 N. Wei, L. Xu, H. Q. Wang, and J. C. Zheng. Strain engineering of thermal conductivity in graphene sheets and nanoribbons: a demonstration of magic flexibility. *Nanotechnology*, 22:105705, 2011.
 - 26 J. Hu, C. Ruan, and Y. P. Chen. Thermal conductivity and thermal rectification in graphene nanoribbons: A molecular dynamics study. *Nano Lett.*, 9:2730, 2009.
 - 27 Enrique Muñoz, Jianxin Lu, and Boris I. Yakobson. Ballistic thermal conductance of graphene ribbons. *Nano Letters*, 10(5):1652–1656, 2010.
 - 28 Z. W. Tan, J. -S. Wang, and C. K. Gan. First-Principles study of heat transport properties of graphene nanoribbons. *Nano Lett.*, 11(1):214, 2011.
 - 29 L. Sun, Q. X. Li, H. Ren, H. B. Su, Q. W. Shi, and J. L. Yang. Strain effect on electronic structures of graphene nanoribbons: A first-principles study. *J. Chem. Phys.*, 129:074704, 2008.
 - 30 Keun Soo Kim, Yue Zhao, Houk Jang, Sang Yoon Lee, Jong Min Kim, Kwang S. Kim, Jong-Hyun Ahn, Philip Kim, Jae-Young Choi, and Byung Hee Hong. Large-scale pattern growth of graphene films for stretchable transparent electrodes. *Nature*, 457:706, 2009.
 - 31 M. Y. Huang, H. G. Yen, C. Y. Chen, D. H. Song, Tony F. Heinz, and J. Hone. Phonon softening and crystallographic orientation of strained graphene studied by raman spectroscopy. *Proc. Nat. Acad. Sci. USA*, 106:7304, 2009.
 - 32 Xiaobo Li, Kurt Maute, Martin L. Dunn, and Ronggui Yang. Strain effects on the thermal conductivity of nanostructures. *Phys. Rev. B*, 81(24):245318, 2010.
 - 33 K. G. S. H. Gunawardana, Kieran Mullen, Jiuning Hu, Yong P. Chen, and Xiulin Ruan. Tunable thermal transport and thermal rectification in strained graphene nanoribbons. *Physical Review B*, 85(24):245417, 2012.
 - 34 H. Sevincli and G. Cuniberti. Enhanced thermoelectric figure of merit in edge-disordered zigzag graphene nanoribbons. *Phys. Rev. B*, 81(11):113401, March 2010.
 - 35 Wu Li, H. Sevincli, G. Cuniberti, and Stephen Roche. Phonon transport in large scale carbon-based disordered materials: Implementation of an efficient order-n and real-space Kubo methodology. *Phys. Rev. B*, 82:041410, 2010.
 - 36 X. Zhai and G. Jin. Stretching-enhanced ballistic thermal conductance in graphene nanoribbons. *Europhys. Lett.*, 96:16002, 2011.
 - 37 Jian -S Wang, Jian Wang, and Nan Zeng. Nonequilibrium Green's function approach to mesoscopic thermal transport. *Phys. Rev. B*, 74(3):033408, 2006.
 - 38 Jian -S Wang, Nan Zeng, Jian Wang, and Chee Kwan Gan. Nonequilibrium Green's function method for thermal transport in junctions. *Phys. Rev. E*, 75(6):061128, 2007.
 - 39 N. Mingo. Anharmonic phonon flow through molecular-sized junctions. *Phys. Rev. B*, 74:125402, 2006.
 - 40 Mads Brandbyge, Jose-Luis Mozos, Pablo Ordejón, Jeremy Taylor, and Kurt Stokbro. Density-functional method for nonequilibrium electron transport. *Phys. Rev. B*, 65:165401, 2002.
 - 41 Zhen Huang, Timothy S. Fisher, and Jayathi Y. Murthy. Simulation of phonon transmission through graphene and graphene nanoribbons with a green's function method. *Journal of Applied Physics*, 108(9):094319, November 2010.
 - 42 C. K. Gan and D. J. Srolovitz. First-principles study of graphene edge properties and flake shapes. *Phys. Rev. B*, 81(12):125445, 2010.
 - 43 Wenzhong Bao, Feng Miao, Zhen Chen, Hang Zhang, Wanyoung Jang, Chris Dames, and Chun Ning Lau. Controlled ripple texturing of suspended graphene and ultrathin graphite membranes. *Nature Nanotechnology*, 4(9):562–566, 2009.
 - 44 Sandeep Kumar, K. P. S. S. Hembram, and Umesh V. Waghmare. Intrinsic buckling strength of graphene: First-principles density functional theory calculations. *Phys. Rev. B*, 82:115411, 2010.
 - 45 T. Markussen, A. -P. Jauho, and Mads Brandbyge. Heat conductance is strongly anisotropic for pristine silicon nanowires. *Nano Lett.*, 8:3771, 2008.
 - 46 L. G. C. Rego and G. Kirczenow. Quantized thermal conductance of dielectric quantum wires. *Phys. Rev. Lett.*, 81:232, 1998.
 - 47 T. Yamamoto, S. Watanabe, and K. Watanabe. Universal features of quantized thermal conductance of carbon nanotubes. *Phys. Rev. Lett.*, 92:075502, 2004.
 - 48 J. Soler, E. Artacho, J. D. Gale, A. García, J. Junquera, P. Ordejón, and D. Sánchez-Portal. The SIESTA method for ab initio order-N materials simulation. *J. Phys.: Condens. Matter*, 14:2745, 2002.
 - 49 Y. W. Son, M. L. Cohen, and Steven G. Louie. Energy gaps in graphene nanoribbons. *Phys. Rev. Lett.*, 97:216803, 2006.
 - 50 G. Kresse, J. Furthmüller, and J. Hafner. Ab initio force constant approach to phonon dispersion relations of diamond and graphite. *Europhys. Lett.*, 32:729, 1995.
 - 51 C. K. Gan, Y. P. Feng, and D. J. Srolovitz. First-principles calculation of the thermodynamics of In(x)Ga(1-x)N alloys: Effect of lattice vibrations. *Phys. Rev. B*, 73:235214, 2006.
 - 52 Y. Y. Zhao, K. T. E. Chua, C. K. Gan, J. Zhang, B. Peng, Z. P. Peng, and Q. H. Xiong. Phonons in Bi2S3 nanostructures: Raman scattering and first-principles studies. *Phys. Rev. B*, 84:205330, 2011.

- ⁵³ Tobias Wassmann, Ari P. Seitsonen, A. Marco Saitta, Michele Lazzeri, and Francesco Mauri. Clar's theory, π -Electron distribution, and geometry of graphene nanoribbons. *J. Am. Chem. Soc.*, 132(10):3440, 2010.
- ⁵⁴ Roland Gillen, Marcel Mohr, Christian Thomsen, and Janina Maultzsch. Vibrational properties of graphene nanoribbons by first-principles calculations. *Phys. Rev. B*, 80(15):155418, 2009.
- ⁵⁵ M. Randic. Aromaticity of polycyclic conjugated hydrocarbons. *Chem. Rev.*, 103(9):3449, 2003.
- ⁵⁶ P. Brocorens, E. Zojer, J. Cornil, Z. Shuai, G. Leising, K. Mllen, and JL Brdas. Theoretical characterization of phenylene-based oligomers, polymers, and dendrimers. *Synth. Met.*, 100(1):141, 1999.
- ⁵⁷ Nicola Bonini, Jivtesh Garg, and Nicola Marzari. Acoustic phonon lifetimes and thermal transport in free-standing and strained graphene. *Nano Letters*, 12(6):2673–2678, June 2012.
- ⁵⁸ R. C. Picu, T. Borca-Tasciuc, and M. C. Pavel. Strain and size effects on heat transport in nanostructures. *J. Appl. Phys.*, 93(6):3535, 2003.
- ⁵⁹ Zhiping Xu and Markus J Buehler. Strain controlled thermomutability of single-walled carbon nanotubes. *Nanotechnology*, 20(18):185701, May 2009.
- ⁶⁰ J. Cai, P. Ruffieux, R. Jaafar, M. Bieri, T. Braun, S. Blankenburg, M. Muoth, A. P Seitsonen, M. Saleh, and X. Feng. Atomically precise bottom-up fabrication of graphene nanoribbons. *Nature*, 466(7305):470, 2010.